Ocean Atmosphere Interaction and Resolution Dependence over the Gulf Stream

Master Thesis

Sebastian Scher

April 2016

Supervisors: Reindert J. Haarsma (KNMI), Aarnout J. van Delden (IMAU)

Acknowledgments

I want to thank my parents for their unconditional support, and Evelien Dekker for helping me to feel at home in the Netherlands.

Note

This master thesis consists of a common introduction, one paper (part I) and one research letter (part II). The manuscript of part I was written by Sebastian Scher, with the other authors contributing to improve it. Part II was written solely by Sebastian Scher.

Contents

Introduction

The Gulf Stream region is one of the worlds major regions of storm-development. It is characterized by strong gradients in Sea Surface Temperatures (SSTs) and a northward extension of warm water along the coast of Florida, the so-called warm tongue. Traditionally, the atmosphere was seen as driving the ocean, and not the other way around. In contrast to this traditional view, there is more and more evidence that the presence of the Gulf Stream has a strong influence on the weather and climate in this region, and also on the weather and climate further away, for example above Europe (e.g.Chang et al. 2002; Czaja & Blunt 2011; Minobe et al. 2008; Small et al. 2014; Booth et al. 2012; Giordani & Caniaux 2001; Jacobs et al. 2008). This new evidence raises the question whether this "driving" of the atmosphere by the ocean is captured by Global Climate Models (GCMs). GCMs are computer models that simulate the climate system, including the atmosphere and the ocean. They usually consist of an atmospheric and an oceanic part, and are widely used both for trying to understand the climate system, and to make projections of the future climate under anthropogenic greenhouse gas forcings. These GCMs do have finite spatial resolution, which has as a consequence that small scale features like the Gulf-Stream SST-front can only partly be captured. Furthermore, the ocean parts of the models are far from perfect. Even if their spatial resolution theoretically would allow to represent the strong SST-gradients of the Gulf Stream accurately, their effective resolution is usually lower due to diffusive effects (e.g. the Gulf Stream is "smeared out") (e.g. Reichler & Kim (2008),Griffies et al. (2015)). Therefore, the atmospheric parts of the models "see" only a weak representation of the Gulf Stream, which might influence the climate in the models and therefore lead to model errors. Consequently, it is necessary to know the influence that a too weak representation of the Gulf Stream has in models. Additionally to the too diffusive ocean models, also the atmosphere has finite horizontal resolution. Therefore, even if the ocean models were prefect (e.g. infinite resolution, no model errors), still the atmospheric part of the model would only see a crude representation of the SST-gradients, because it has to average the SST-fields to its own (coarse) resolution. Accordingly a question arises: how high must the horizontal resolution of the atmosphere be to accurately capture all effects induced by fine details of the Gulf Stream? This leads us to our first question: how do current GCMs - with current operational horizontal resolutions - perform above the Gulf Stream? Does an increase in horizontal resolution lead to significant differences in the performance? This will be addressed in the first part if this thesis.

In the second part, we will look in more detail at the interaction between the ocean and the atmosphere in the Gulf Stream region, and we will assess how individual storms are influenced by the presence of the Gulf Stream.

References

Booth, J. F., Thompson, L., Patoux, J., & Kelly, K. A. (2012). Sensitivity of midlatitude storm intensification to perturbations in the sea surface temperature near the gulf stream. *Monthly Weather Review*, 140(4), 1241–1256.

Chang, E. K., Lee, S., & Swanson, K. L. (2002). Storm track dynamics. *Journal of Climate*, 15(16), 2163–2183.

Czaja, A. & Blunt, N. (2011). A new mechanism for ocean–atmosphere coupling in midlatitudes. *Quarterly Journal of the Royal Meteorological Society*, 137(657), 1095–1101.

Giordani, H. & Caniaux, G. (2001). Sensitivity of cyclogenesis to sea surface temperature in the northwestern atlantic. *Monthly weather review*, 129(6), 1273–1295.

Griffies, S. M., Winton, M., Anderson, W. G., Benson, R., Delworth, T. L., Dufour, C. O., Dunne, J. P., Goddard, P., Morrison, A. K., Rosati, A., Wittenberg, A. T., Yin, J., & Zhang, R. (2015). Impacts on ocean heat from transient mesoscale eddies in a hierarchy of climate models. *Journal of Climate*, 28(3), 952–977.

Jacobs, N., Raman, S., Lackmann, G., & Childs Jr, P. (2008). The influence of the gulf stream induced sst gradients on the us east coast winter storm of 24–25 january 2000. *International Journal of Remote Sensing*, 29(21), 6145–6174.

Ma, X., Chang, P., Saravanan, R., Montuoro, R., Hsieh, J.-S., Wu, D., Lin, X., Wu, L., & Jing, Z. (2015). Distant influence of kuroshio eddies on north pacific weather patterns? *Scientific reports*, 5.

Minobe, S., Kuwano-Yoshida, A., Komori, N., Xie, S.-P., & Small, R. J. (2008). Influence of the gulf stream on the troposphere. *Nature*, 452(7184), 206–209.

Reichler, T. & Kim, J. (2008). How well do coupled models simulate today's climate? *Bulletin of the American Meteorological Society*, 89(3), 303–311.

Small, R. J., Tomas, R. A., & Bryan, F. O. (2014). Storm track response to ocean fronts in a global high-resolution climate model. *Climate dynamics*, 43(3-4), 805–828.

Part I

Resolution Dependence of Precipitation and Deep Convection over the Gulf Stream

Sebastian Scher[1,2],
Reindert J. Haarsma[2], Sybren S. Drijfhout[1,2,3], Hylke de Vries[1], Aarnout J. van Delden[2]

Abstract

The influence of horizontal resolution of an Atmospheric Global Circulation Model on the simulation of precipitation and atmospheric deep convection above the North Atlantic and especially the Gulf Stream region is studied. It is shown that mean precipitation increases with increasing resolution. This result is confirmed with reanalyses and weather forecasts using different resolutions, ranging from 125 to 16 km. Via an analysis of the position of the jetstream it is suggested that the differences in mean precipitation in the GCM are not caused by differences in large scale circulation, but mainly by local phenomena. Increasing resolution in the GCM especially leads to more extreme precipitation. This also occurs in reanalyses and operational analyses. An assessment whether the increase in extreme precipitation deteriorates or improves model performance appears impossible as it depends on which observational product is used. Furthermore, 10m wind convergence has been analyzed and it is shown that the higher resolution GCM shows more extreme wind convergence events and corresponds better to wind convergence derived from observations. Additionally, the number of deep convection events above the Gulf Stream increases with resolution in GCMs, reanalyses and operational forecasts, enhancing the communication of Sea Surface Temperatures up to the troposphere.

1 Introduction

Global Climate Models (GCMs) are widely used for simulating the earth's climate and to make projections of future climate under different forcings. State of the art GCMs are typically run at a spatial resolution of ∼100km. These models capture the current climate well in terms of temperature, but less so in in terms of spatial precipitation patterns (Flato et al. 2013). Models across a wide range of types and resolution show too high frequency of precipitation events and too little intensity (Stephens et al. 2010).

In midlatitudes precipitation is tightly coupled to position and intensity of storm tracks. Climate models with high spatial resolution perform better in simulating the North Atlantic storm track than models with lower resolution (Zappa et al. 2013, Colle et al. 2013). Increasing model resolution in the same model as used in the current study improved precipitation performance above Europe (van Haren et al. 2015).

[1]Institute for Marine and Atmospheric Research (IMAU), Utrecht University, Utrecht, The Netherlands
[2]Royal Dutch Meteorological Institute (KNMI), De Bilt, The Netherlands
[3]Ocean and Earth Science, National Oceanography Centre Southampton, University of Southampton, United Kindgdom

Whereas precipitation is a relevant parameter for a variety of applications (e.g. projections of changes in hydrology, agriculture etc.), vertical motion - to which precipitation is closely linked - gives a better insight in the dynamical properties of the models. Czaja & Blunt (2011) showed with theoretical considerations and reanalysis data that in midlatitudes above oceanic boundary currents convection through the whole troposphere can occur, allowing the Sea Surface Temperatures (SSTs) to be communicated through the whole troposphere. This type of strong convection could be important for the high tail of precipitation distributions. Therefore, the capturing of these convective events by models might be crucial for precipitation performance. Further it is known that the sharp SST-fronts occurring together with boundary currents in the ocean have a significant impact on storm tracks and precipitation (Small et al. 2014, Minobe et al. 2008). An atmospheric model with low spatial resolution "sees" only a very crude representation of these SST-fronts and eddies, therefore increasing model resolution might also change precipitation and convection indirectly through better resolved ocean-atmosphere interaction. One such area where SST-fronts impact storm tracks is the Gulf Stream region. Recent studies have shown that small scale SST variability in the Gulfstream region affects the atmospheric circulation (Ma et al. 2015), although the mechanisms responsible for this ocean to atmosphere forcing are still unresolved. The Gulfstream front is the genesis region for the mid-latitude storms that are fueled by baroclinic instability. However, in the initial stage of the storms, the forcing by the ocean affecting the vertical movement and the release of latent heat caused by precipitation plays an important role. Crucial questions are how increasing resolution affects this type of interaction and, if so, whether it results in an improvement compared with observations.

To address these questions the present study is focused on wintertime (DJF), when storm track activity is highest. The area we analyze is the North Atlantic, particularly the Gulf Stream region (see black rectangle in fig. 1). In particular we have divided our overarching research question in five more detailed questions: (1) whether and how spatial model resolution, and especially the increase to very high resolution (∼25 km), affects precipitation, (2) whether these potential differences in precipitation are caused by differences in large scale circulation or by local phenomena, (3) whether precipitation performance is increased with higher resolution, (4) whether deep convection through the whole troposphere occurs in the models analysed and (5) the resolution dependence of this occurrence.

2 Data

Two runs with different resolution were made with the atmosphere-only part of the GCM EC-Earth. EC-Earth is a state-of-the art climate model, based on the Integrated Forecast System (IFS) from ECMWF (see Hazeleger et al., 2012). Each of the two runs consists of six ensemble members, where each member is run for five years (2002-2006), thus comprising 30 years for each resolution. The two runs differ only in resolution of the model, with all other settings kept the same. The low resolution model has a spectral resolution of T159L62, corresponding to approximately 1.1 degrees or 125 km with 62 vertical layers, while the high resolution model has a spectral resolution of T799L91, corresponding to approximately 0.25 degrees or 28 km with 91 vertical layers. Due to storage limitations only 5 (pressure-)levels of saved data are available. For a more detailed description of the runs see Haarsma et al. (2013). We shall from now on refer to the low resolution run as EC-Earth T159, and to the high resolution run as EC-Earth T799. The external forcing consists of prescribed greenhouse gas concentrations and prescribed fields of sea surface temperatures (SSTs) and sea ice concentrations. As SST and sea ice data version 2 of the NOAA 1/4° daily Optimum

Interpolation Sea Surface Temperature data set (Reynolds et al., 2007) was used. For validation, the model datasets are compared to two reanalysis datasets (ERA-Interim and MERRA), and operational analyses from ECMWF (hereafter referred to as ECMWF-operational).

ERA-Interim (Dee et al., 2011) is a reanalysis dataset from 1979 to present, based on IFS with a spectral resolution of T255 (approx. 0.75 degrees) and time resolution of 6 hours. It uses the same IFS-configuration as the ECMWF-operational analysis from year 2006 (Cy31r2), but with lower horizontal resolution. MERRA (Modern Era Retrospective-Analysis for Research) is a reanalysis dataset provided by NASA (Rienecker et al., 2011). It is based on the Goddard Earth Observing System and focuses on the hydrological cycle. The motivation for including MERRA is that it is not based on the IFS. For monthly mean precipitation, the monthly version or the GPCPv2.2 precipitation dataset (Adler et al., 2003) was used for the period 1985-2014. GPCP is a merged analysis of low-orbit satellite microwave data, geostationary satellite infrared data and rain-gauges (the latter play only an indirect role as calibration in our study area). GPCPv2.2 has a resolution of 2.5x 2.5 degrees. For daily analyses, both the daily version of GPCPv2.2, and the CMORPH0.5 dataset (Joyce et al., 2004)) were used for the period 1997-2014. CMORPH has a spatial resolution of 0.25 x 0.25 degrees.

For surface wind observations, the satellite observations from the Cross-Calibrated Multi-Platform Ocean Surface Wind Vector L3.0 First-Look Analyses (CCMP) for the period 1988-2011 were used (Atlas et al., 2011).

If not otherwise noted, all data have been regridded to the T159 grid by means of second order conservative remapping (Jones, 1999).

3 Results

3.1 Precipitation

In this section precipitation performance of EC-Earth is assessed and the impact of increasing resolution from T159 to T799 is discussed. The performance is compared to operational analyses and reanalyses, and we analyze whether the differences are caused by differences in large scale circulation or by local phenomena such as convection.

Figure 1 shows average DJF precipitation for all 30 years of the EC-Earth T159 simulation and the difference between EC-Earth T799 and EC-Earth T159. Both model configurations perform very similarly, but T799 EC-Earth produces more ($\sim$1mm/day) precipitation east off the east coast of the US. While there is a slight increase of the 'hot-spot' of precipitation located around 40N -60E at T799, the biggest absolute difference as well as the biggest relative difference (not shown) is situated south of this region. The difference between T159 and T799 resolutions consists of a dipole pattern, with less precipitation at T799 north of the Gulf Stream, and more to the south of it. This result corresponds to the storm track analysis of van Haren et al. (2015), who found for the same dataset a weakening of the storm track north of the Gulf Stream with increasing resolution. It should be noted that van Haren et al. showed that the simulated storm track of T159 corresponds better to ERA-Interim in this region than the one from T799.

To test whether the precipitation difference is caused by local phenomena or by differences in the large scale circulation, we analyzed the position of the jetstream. Traditional jetstream measures, like the time mean of 300hPa windspeed make it difficult to separate differences in position of the jetstream and its speed. Therefore, we defined the jetstream as the meridional position of the maximum wind speed at 300hPa between 27N and 90N, analyzed in 6hour-timesteps.

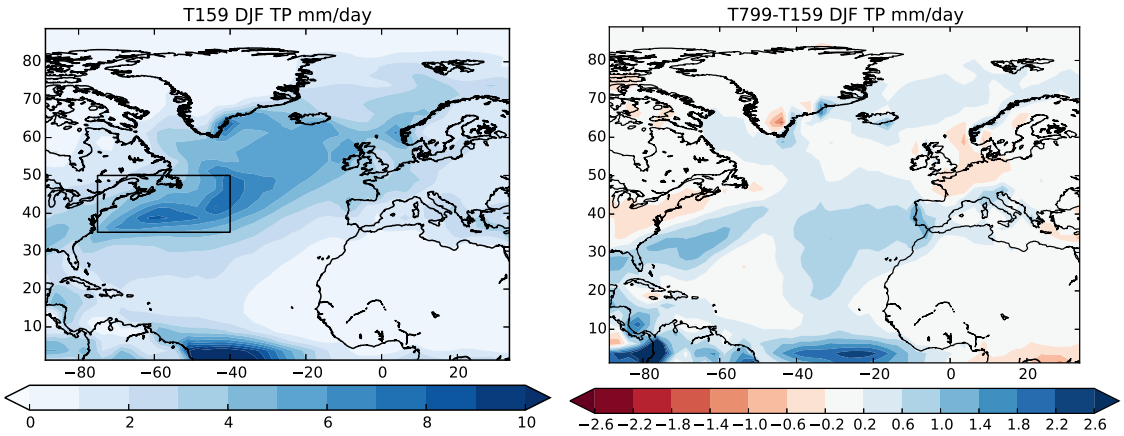

Figure 1: Wintertime rainfall for the present climate for EC-Earth T159 (left) and difference between T799 and T159 (right). The black rectangle denotes the study region.

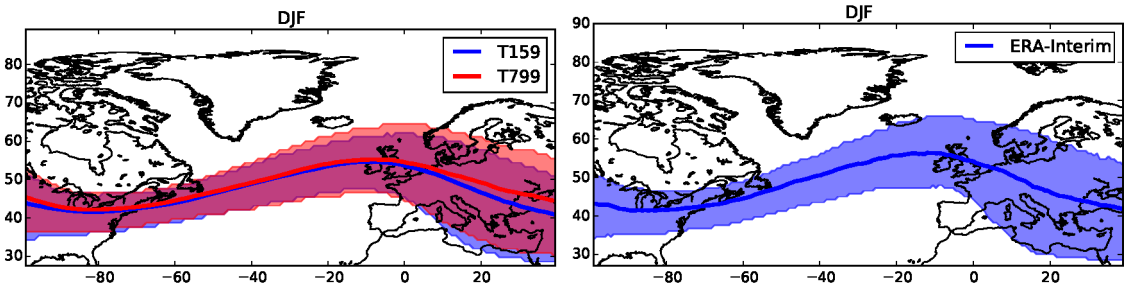

(a) EC-Earth (b) ERA-Interim

Figure 2: Location of the wintertime jetstream at 300hPa. Line denotes the mean and shading the 25-75% range of the position

Figure 2 shows the mean wintertime location and the 25-75% range of the jetstream position in both models and in ERA-Interim. Both model versions show a realistic representation of the jetstream position. At lower resolution EC-Earth shows slightly less spread than ERA-Interim in the eastern part of the North Atlantic and over Europe, while at high resolution EC-Earth has nearly the same spread as ERA-Interim. Above Eastern Europe the EC-Earth T799 has a northward shift compared to ERA-Interim and EC-Earth T159. Over the North Atlantic and especially our study region the differences between the two model resolutions are negligible, and both models capture the position of the jet stream very well, indicating that the planetary wave structure is correctly simulated at both resolutions. This suggests that the weakening of the storm track north of the Gulf Stream, found by van Haren et al., and the associated changes in precipitation shown in fig. 3.1 are more related to local processes and not primarily induced by changes in the large scale circulation.

We proceed by comparing the model data to precipitation observations. The setup of using the SST-forcing from 2002-2006 for five members makes an exact comparison with observational data impossible, as the five years of observations from 2002-2006 are only one of the possible realizations of the climate with this SST-forcing. Here we used 30 years of observations as reference. The additional precipitation that T799 produces south of the Gulf Stream matches better to GPCPv2.2 observations (see fig. 3 a and b). However, at around 40N 50W, T799 shows an overestimation

compared to GPCPv2.2. Averaged over the study region, T799 has a higher spatial Root Mean Square Error (RMSE) than T159 (0.87 mm/day compared to 0.67 mm/day). This difference in RMSE has been shown to be statistically significant by analyzing each of the six ensemble members separately. For each ensemble member, the T799 version has higher RMSE than T159. The difference is also robust to changes of the exact definition of the study region. Therefore, in the study region the performance of mean precipitation significantly decreases with increasing resolution in the EC-Earth experiment. When comparing the mean amount of precipitation in the study area, T799 produces more precipitation (5.45 mm/day) than T159 (5.28 mm/day). Thus increasing resolution leads to more precipitation.
Fig. 3c shows ERA-Interim precipitation compared to GPCPv2.2. The error pattern more closely resembles the one from T159 than from T799. We remind that ERA-interim is based on IFS with a resolution of T255. Interestingly the MERRA reanalysis produces a similar error pattern as ERA-interim, but with stronger negative biases in the study area (and at all mid-latitudes), producing too little precipitation. This is a known deficiency of MERRA (Rienecker et al. 2011). A common feature occurring in the different resolutions of IFS and the reanalyses is a spot of underestimation close to the coast of New York. The magnitude of underestimation of this spot is very similar for EC-Earth T159, T799 and ERA-Interim, and stronger for MERRA. For the ECMWF operational analysis it is highly resolution dependent (see below). The origin of this spot is unclear and might be related to local topographic effects (e.g Appalachians and land-sea contrast) that need even higher resolution to be simulated adequately, or it might be caused by a deficiency in the observations.

To further examine the effect of horizontal resolution on precipitation rates, the ECMWF operational dataset has been split up over time according to the resolution changes of the forecast model. This provides five different resolutions (T106, T213, T319, T799 and T1279). Because the highest two resolutions span only a period of four years each, they have been grouped together to form one period of eight years for higher statistical significance. Not the exact date of the change in resolution has been used, but the 1st of January from the year in which the resolution update occured. This ensures that every timespan consists of an exact multiple of three months. Fig. 4 shows the difference between these four datasets and GPCP. Precipitation performance in the study area increases significantly with each step in resolution. T106 shows a strong underestimation in the whole study area. In T213 this underestimation is weaker. T319 shows a dipole pattern of under and overestimation, with absolute errors lower than T213. T799 and T2179 also show a dipole pattern, but weaker than T319. Thus, with each step of increasing resolution, precipitation performance becomes better, which in the northern region of the Gulf Stream is accomplished with increasing the precipitation produced by the model (thus getting less underestimation). While an exact pinning down to resolution differences is not possible, as also other components of the ECMWF model besides changed over time, this further strengthens the conclusion from the EC-Earth experiment that higher resolution increases precipitation amounts, especially for models based on the IFS.

Extreme Events

Investigating extreme precipitation events yields even larger differences between different resolutions. Fig. 5 shows the fraction of winterdays with more than 30 mm precipitation for EC-Earth T159 and T799. There is a clear increase in frequency with higher resolution, especially above the Gulf Stream.

A more detailed picture can be gained from fig. 6, which shows histograms of daily precipitation

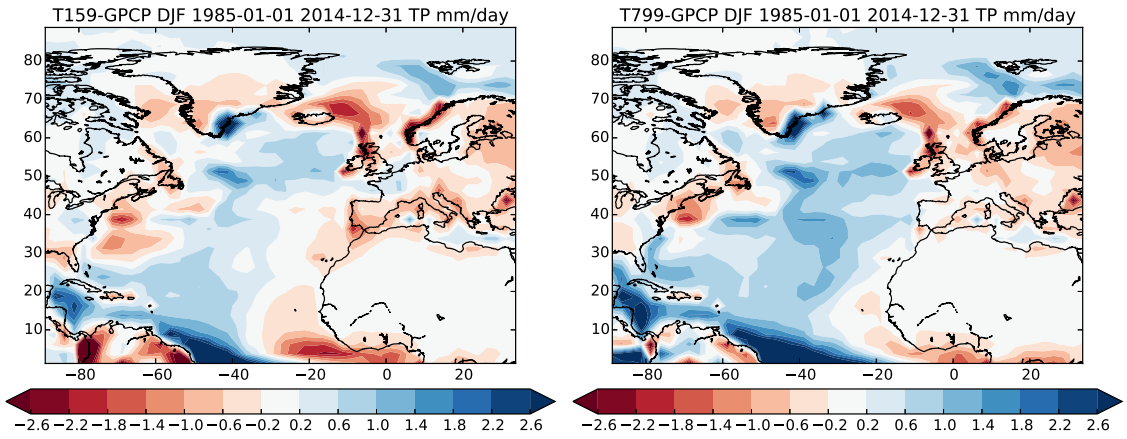

(a) T159

(b) T799

(c) ERA-Interim

(d) MERRA

Figure 3: Comparison of simulated wintertime precipitation and observations from GPCPv2.2 for the medium and high resolution GCM and two reanalysis-datasets. Model data were regridded to GCPCv2.2 grid

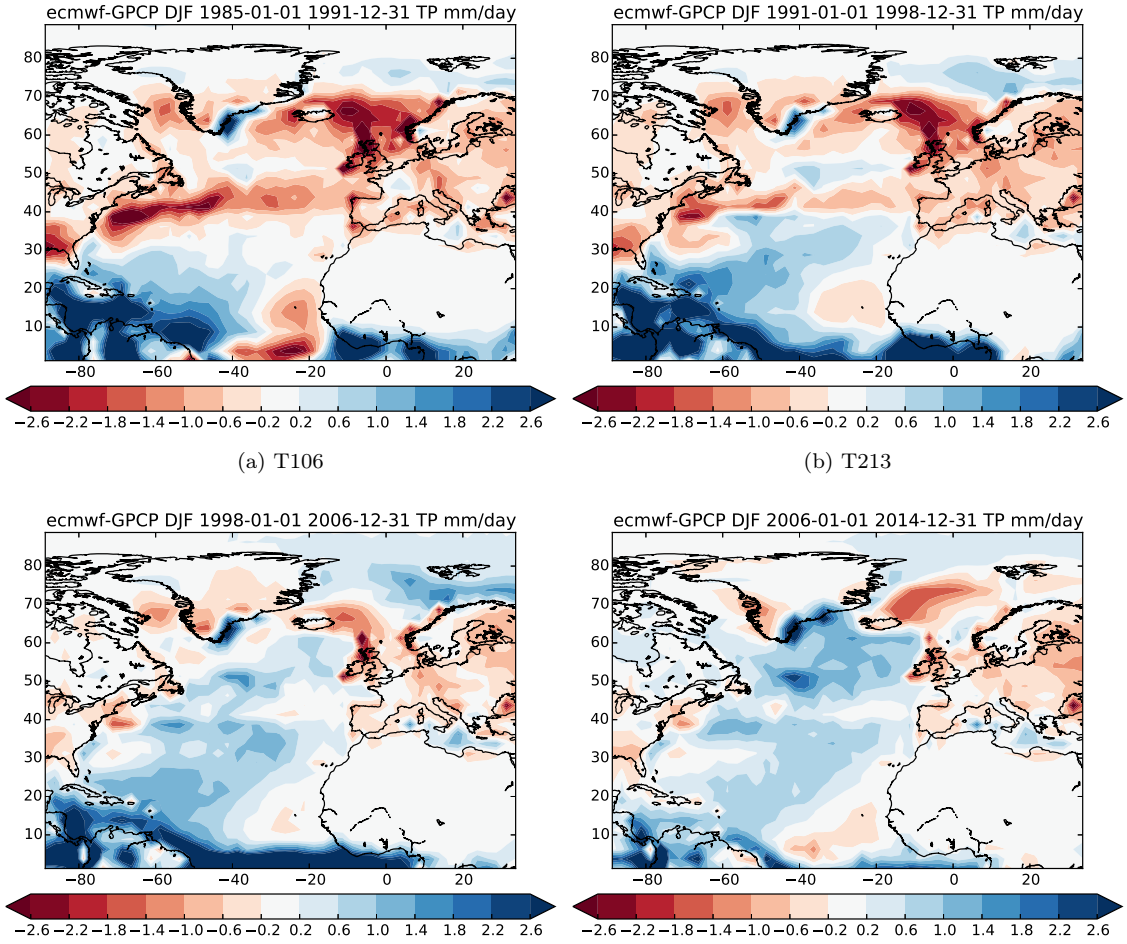

(a) T106 (b) T213

(c) T319 (d) T799 (4 yeras) and T1279 (4 years)

Figure 4: Difference between ECMWF operational analysis wintertime precipitation and GPCPv2.2 observations. Shown are four time-periods, that were chosen such that in each timeperiod the operational model had a fixed horizontal resolution. (for homegenity the timeperiods always start at 1 January and end at 31 December, eventhough the resolution might have been chagned in a different month)

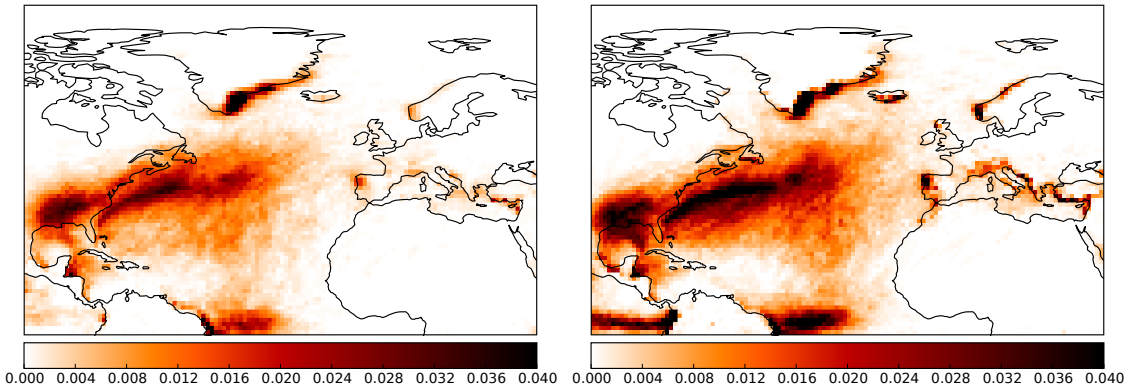

(a) T159 (b) T799

Figure 5: Fraction of wintertime extreme precipitation events (> 30 mm/day) for a) the medium resolution and b) the high resolution version of EC-Earth

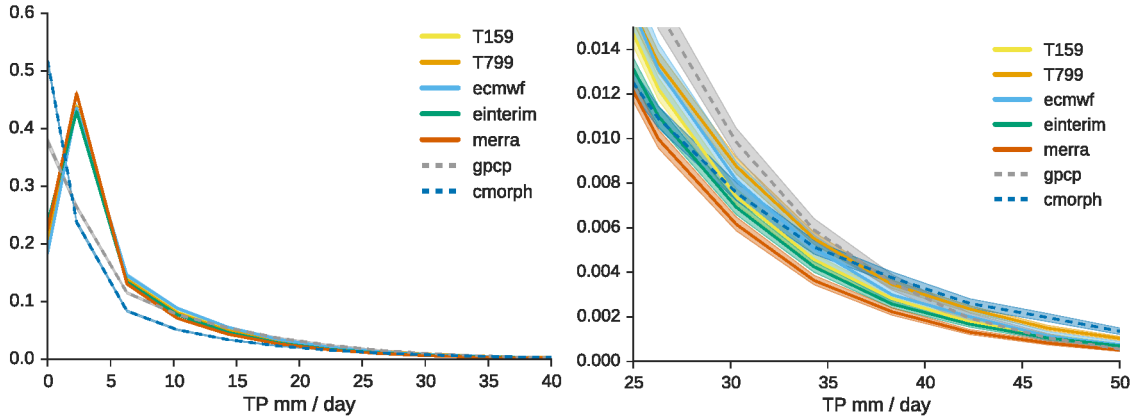

Figure 6: Distribution of wintertime daily rainfall events in the study area for EC-Earth T159 and T799, MERRA reanalysis, ECMWF-operational analysis and GPCPv2.2 observations. Reanalyses from 1985-2014, observations from 1997-2014, ECWMF-operational from 2006-2014 (T799 and T1279). Both plots show the same data but with different scales. The range indicates the 5-95% confidence interval estimated with bootstrapping. y-axis denotes fraction of wintertime days.

over the study area. The 5-95% confidence ranges were computed with bootstrapping daily events. All models and (re)-analyses show significantly less dry days, and more days with low rainfall amounts (<6mm/day) than observations. This might be caused by a deficiency in the observations, which use infrared satellite data which are known to underestimate low precipitation (see Joyce et al. (2004) for CMORPH and Adler et al. (2003) for GPCP). On the other hand, models are known to simulate too many drizzle days (drizzle effect) (e.g. Stephens et al. 2010). Therefore, no solid conclusions can be drawn from this part of the rainfall distribution. On the high-rainfall side of the distribution we see that EC-Earth T799 (orange line) shows more events from 25 mm/day upwards than EC-Earth T159 (yellow line).Thus, increasing the resolution of EC-Earth leads to more strong precipitation events, as already illustrated in fig. 5. The ECMWF-operational analyses from 2006-2014 (T799 and T1279) shows an even extremer distribution than EC-Earth T799, with fewer events for rainfall amounts lower than 38 mm/day and more events for rainfall amounts higher than 38 mm/day. This strengthens the conclusion that higher resolution leads to stronger precipitation events. ERA-Interim shows less extreme events than EC-Earth at T159 and at T799 and the ECMWF-operational analysis. While this is surprising at first sight, it can be explained by the configurational details of ERA-Interim. ERA-Interim uses IFS cycle Cy31r1. The IFS model underwent a change in the cloud scheme in cycle Cy25r3 (made operational on 14 Jan 2003), which made the atmosphere more stable, leading to less vertical motion and thus less precipitation (Dee et al. 2011). ERA-Interim uses this more stable cloud scheme, but at a resolution of only T255, thus having a combination of relatively low resolution and the new stable cloud scheme. This explains the low amount of high precipitation events compared to the EC-Earth simulations and the ECMWF-operational analysis. Furthermore, this also strengthens the conclusion of higher extreme precipitation rates with resolution, as ERA-Interim uses a very similar model configuration as the ECMWF-operational analysis from 2006-2014 shown in fig. 6, but at lower resolution.

Comparison of the models and (re-)analyses with two observational datasets (dashed lines in fig 6) reveals that the CMORPH-dataset shows more precipitation events >38 mm/day than all models and (re-)analyses. The GPCP dataset shows less dry days than CMORPH, more events between 4 mm/day and 38 mm/day, and fewer events >38 mm/day. Thus, at the high-end tail of the

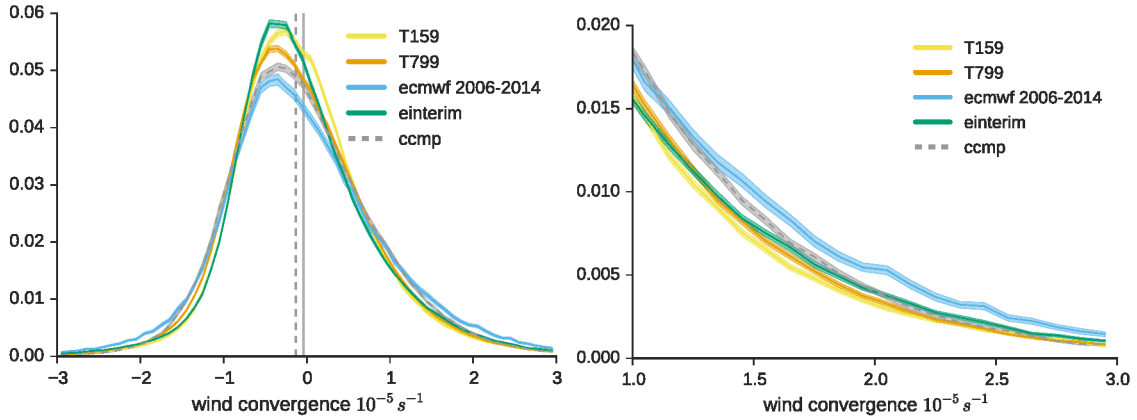

Figure 7: As fig. 6, but for wintertime daily mean wind convergence. The vertical lines denotes the median (dashed) and the mean (solid) of wind convergence derived from wind observations (CCMP). y-axis denotes fraction of wintertime days.

distribution, the GPCP dataset lies between EC-Earth T159 and T799. As we are not able to judge which of the two datasets is more valid for our analysis, we are not able to make a conclusion which of the two EC-Earth resolutions performs better, and how this compares to reanalyses and the ECMWF operational analysis. This does, however, not impair our findings of increased extreme precipitation with increasing resolution, shown both by the EC-Earth experiment and comparing ERA-interim with the ECMWF-operational analysis.
The patterns described here are the same for summer precipitation, with all thresholds moved to lower precipitation amounts (not shown).

3.2 Wind Convergence

As a measure of convective activity, we also investigated the distribution of vertical velocity. As no direct measurements of vertical velocity are available, we used horizontal wind divergence at a height of 10 m (calculated with centered differences from 10m wind-components) as a proxy for vertical velocity. Fig. 7 shows the distribution of daily mean wind convergence events at 10m above the study area for EC-Earth T159, EC-Earth T799, ECMWF-operational, ERA-Interim and observations (CCMP, see data section). For all models and observations, the distribution is skewed to negative values (diverging wind), but the mean and median (vertical lines in fig. 7) of the events are very close to zero. Thus even though the most frequent event is a divergence event, this is compensated by a wider distribution at the right-hand (convergence) side of the distribution.

The tails of the distribution show a diverse pattern. Two striking features are that EC-Earth T159 has a narrower (less extreme convergence/divergence events) distribution than T799, and that ECMWF operational has a significantly broader distribution (more extreme convergence/divergence events) than all other models and observations. ERA-Interim features slightly more extreme events than both versions of EC-Earth. The observations show less extreme divergence ($< -2 \cdot 10^{-5} s^{-1}$) events than all models (not visible in fig. 7 because of the scaling of the figure), and approximately the same amount of extreme convergence ($> 2 \cdot 10^{-5} s^{-1}$) events as EC-Earth T159 and T799. The fact that the ECMWF operational analysis shows a more extreme distribution than all other models and observations means that - assuming the observations are accurate - the very high resolution operational analyses over-estimates high wind-convergence events. Because the analyses shown here are for different time-periods, the comparison between

ECMWF operational analysis and observations has been repeated for the overlapping period of 2006-2011, which confirms the too strong high wind-convergence of the ECMWF operational analysis (not shown). Summarizing, we conclude that the 10m wind convergence pattern is similar to the precipitation analysis, with the ECMWF-operational analysis showing the highest frequency of strong convergence events, followed by EC-Earth T799 and T159. ERA-Interim, in contrast to its precipitation-performance, shows more strong wind convergence events than both resolutions of EC-Earth and sits in between EC-Earth and the ECMWF-operational analysis. The difference between IFS T159 and T799, and especially the pronounced difference between ERA-Interim and the ECMWF-operational analysis imply that higher resolution leads to more strong wind convergence events. Why ERA-interim simulates more strong wind-convergence events than IFS T799 is unclear but might be related to the data assimilation scheme.

3.3 Deep Convection

Deep convection throughout the troposphere up to the tropopause is common in specific tropical regions such along the ITCZ and the Pacific warm pool. However Czaja & Blunt (2011) showed that if certain criteria are fulfilled - namely that the moist entropy of air at the ground equals or exceeds the moist entropy at the tropopause - deep atmospheric convection can occur above oceanic boundary currents. To detect deep convection, it was investigated how often vertical velocity at all pressure levels between 850hPa and 300hPa (comprising of 4 levels in the available data) above a gridpoint at the ground exceeds a certain threshold. To identify slantwise convection (according to Czaja & Blunt occurring more often than straight upward convection), the criterion we used also allowed for going to a horizontal neighbor gridpoint with each new level. All data was analyzed on the T159 grid. Since the threshold is arbitrary, the analysis was repeated with several thresholds. 6-Hourly data was used. Fig. 8 shows the results for DJF with a threshold of -0.2 Pa/s. Even though the fraction of days where the criterion is met rises with lowering the threshold, the basic pattern is always the same, with most events occurring in regions of high SSTs and the Gulf Stream being clearly visible. Although we used a different diagnostic for deep convection than Czaja & Blunt (2011) because of the limited vertical resolution (5 pressure levels) of available model data, our results reveal a similar pattern as in Czaja & Blunt (2011). The very high values on the coast of Greenland are caused by orographic convection and are not discussed. Fig. 9 shows the mean fractions above the study region for two thresholds (-0.2 Pa/s and -0.5 Pa/s), ordered by resolution on the x-axis. EC-Earth T799 shows more events than EC-Earth T159 for both thresholds. The ECMWF operational analysis from 2006-2014 (T799 and T1279) has the highest fractions with both thresholds. For -0.5 Pa/s, the fraction of ERA-Interim - with a resolution of T255 lying between EC-Earth T159 and EC-Earth T799) - is between the fraction in EC-Earth T159 and EC-Earth T799 (left panel in fig. 9). Thus at this threshold, we have a positive correlation between horizontal resolution and the fraction of deep convection events. For the threshold of -0.2 Pa/s, the results are slightly different (right panel in fig. 9). Here ERA-Interim lies outside the line, showing less events of deep convection than EC-Earth T159. This is caused by the more stable characteristics of ERA-Interim already mentioned in section 3.1, and does not affect our findings. For a more extensive discussion of this issue we refer to the supplementary material.

The analysis has been repeated over the Northern Pacific. Here the Kuroshio boundary current is clearly visible in the pattern of fractions of deep convection events. These fractions also increase with resolution (not shown). Due to the absence of direct measurements of vertical velocity and the fact that vertical velocity in reanalysis is strongly model dependent, it cannot be judged which of the model versions and /reanalyses corresponds best to reality. Nevertheless, it can be concluded

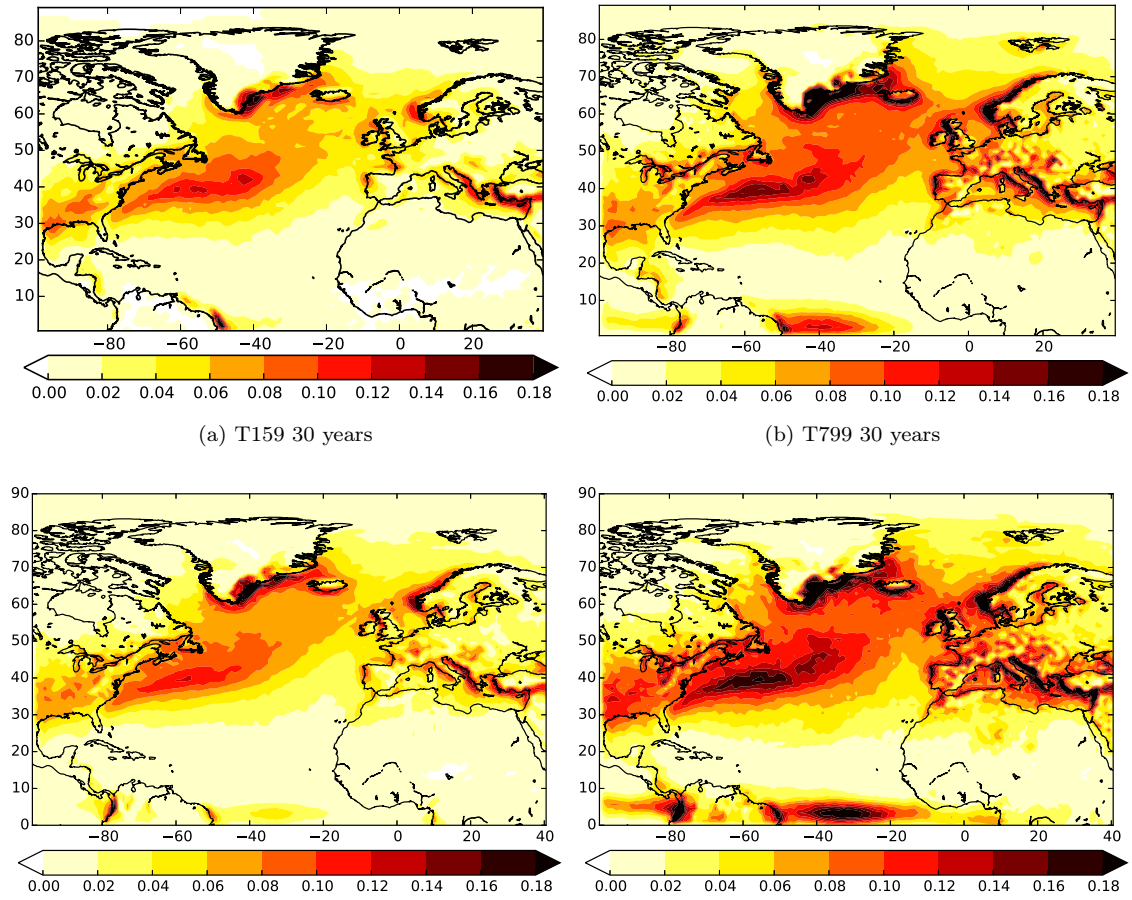

(a) T159 30 years

(b) T799 30 years

(c) ERA-Interim 1985-2014

(d) ECMWF operational 2006-2014

Figure 8: Fraction of wintertime deep convection events (ω < -0.2 hPa/s from 850-300 hPa, for details see text)

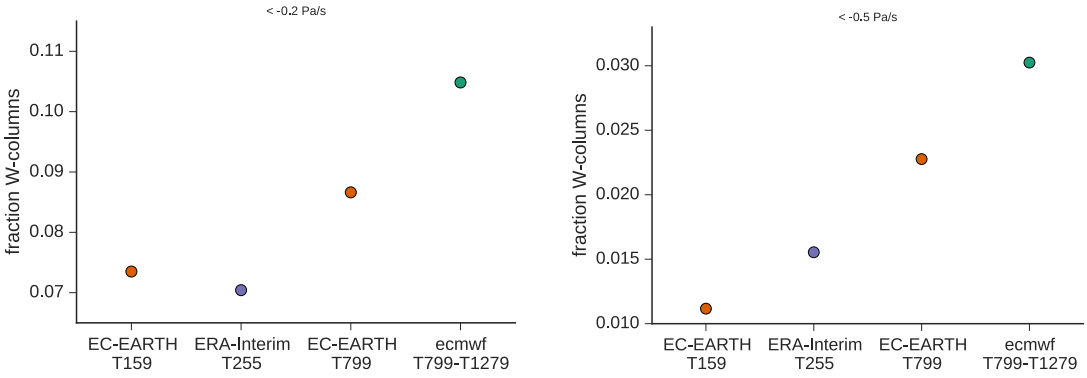

Figure 9: Fraction of wintertime events of deep convection (ω < threshold from 850-300 hPa, details see text), with threshold -0.5 Pa/s (left) and -0.2 Pa/s (right), averaged over the study region. x-axis shows spectral horizontal resolution of the model/renalalysis. ECMWF-operational (denoted ecmwf) was split up in four time-periods, corresponding to periods with a certain horizontal resolution. Note that the x-axis is only categorical and not exactly scaled to horizontal resolution.

that higher resolution leads to more deep convection events. This strengthens the assumption made in section 3.1 that the difference (mainly strengthening) of precipitation in the study region is caused by local phenomena associated with vertical ascent and convection.

To further investigate the characteristics of deep convection we compared the fraction of days where the criterion is met at 850 hPa to the fraction of days on which it is met in the whole column (note that the first criterion pass is a necessary condition for the latter pass). For a threshold of -0.2 Pa/s (as used above) around 80% of the convective events at 850hPa are accompanied by a a whole column of convective events, independent of model and/or resolution. For a threshold of -1.0 Pa/s, both for EC-Earth T159 and ERA-Interim, between 10-20% of the convective events at 850hPa are accompanied with a whole column of convective events. For EC-Earth T799 this fraction is larger (around 40%), ECMWF operational (T799 and T1279) shows even slightly higher fractions than EC-Earth T799. Thus, the fraction of ground convection events that translate to a convection event in the whole column is only dependent on resolution for events with threshold -1.0 Pa/s. For these strong events, the fraction increases with increasing resolution. Independent of the threshold and the model version or reanalysis, the fraction is slightly higher just northwards of the Gulf Stream. One possible explanation could be an influence of the SST-gradients, which are largest in this region. However, the region of larger deep convection/ground convection fractions does not coincide with the region of the highest potential for deep convection (Czaja & Blunt, 2011). This renders an influence of SST-gradients more unlikely, but it cannot be ruled out either. Another explanation might be related to the land-sea contrast: dry easterly cold continental air that comes in contact with the warm moist ocean will significantly increase its entropy, thereby enhancing the possibility of deep convection. From the available data it cannot be concluded which of the two explanations is the most likely, nor what the details are of the driving mechanisms.

4 Summary and Conclusions

We assessed the impact of spatial model resolution on precipitation and vertical motion using climate simulations, reanalysis and operational forecasts. The region of focus was the the Gulf Stream region, which is a source region for cyclogenesis. Our analysis indicates that resolution dependent changes in mean precipitation patterns over that region are not primarily caused by changes in the large-scale circulation, such as the position of the storm track, but by local processes related to vertical ascent and deep convection. The impact of resolution becomes more prominent in the high-end tails of the precipitation distribution. Increasing resolution results in more dry days and more intense precipitation events. A rigorous evaluation whether these changes represent an improvement could not be made due to the lack of reliable observations over the ocean. For the tails in the distribution of precipitation the available satellite products showed ambiguous results and could not be checked with other ground based observations. Nevertheless, we argue that due to the small scale of the crucial processes, increasing resolution is beneficial for a correct simulation of precipitation. This is supported by the improvement of the precipitation patterns with resolution for the operational forecasts/ reanalysis. However, due to the dependence of precipitation on unresolved processes like turbulent heat fluxes and cloud formation, which have to be parameterized, our analysis also revealed that enhanced resolution does not necessarily result in an improvement for all regions. The increase of extreme precipitation events was accompanied by enhanced wind convergence and deep convection, of which the former could be verified by observations and the latter agrees with theoretical arguments put forward by Czaja & Blunt (2011).

In conclusion we state that over the studied area there is a strong dependence of in particular extreme rainfall, vertical movement and deep convection on model resolution. Although, due to lack of reliable observations we cannot judge what minimal resolution is required for a correct simulation, the lack of saturation of extreme rainfall with resolution suggests that even higher resolution than present NWP models is required.

Data Sources

GPCP Precipitation data provided by the NOAA/OAR/ESRL PSD, Boulder, Colorado, USA, from their Web site at http://www.esrl.noaa.gov/psd/

CMORPH data obtained via Climate Explorer (https://climexp.knmi.nl/)

Acknowledgments

This paper was partly funded by the PRIMAVERA project under Grand Agreement 641727 in the European Comission's Horizon 2020 research program.

References

Adler, R. F., Huffman, G. J., Chang, A., Ferraro, R., Xie, P.-P., Janowiak, J., Rudolf, B., Schneider, U., Curtis, S., Bolvin, D., et al. (2003). The version-2 global precipitation climatology project (gpcp) monthly precipitation analysis (1979-present). *Journal of hydrometeorology*, 4(6), 1147–1167.

Atlas, R., Hoffman, R. N., Ardizzone, J., Leidner, S. M., Jusem, J. C., Smith, D. K., & Gombos, D. (2011). A cross-calibrated, multiplatform ocean surface wind velocity product for meteorological and oceanographic applications. *Bulletin of the American Meteorological Society*, 92(2), 157–174.

Booth, J. F., Thompson, L., Patoux, J., & Kelly, K. A. (2012). Sensitivity of midlatitude storm intensification to perturbations in the sea surface temperature near the gulf stream. *Monthly Weather Review*, 140(4), 1241–1256.

Chang, E. K., Lee, S., & Swanson, K. L. (2002). Storm track dynamics. *Journal of Climate*, 15(16), 2163–2183.

Colle, B. A., Zhang, Z., Lombardo, K. A., Chang, E., Liu, P., & Zhang, M. (2013). Historical evaluation and future prediction of eastern north american and western atlantic extratropical cyclones in the cmip5 models during the cool season. *Journal of Climate*, 26(18), 6882–6903.

Czaja, A. & Blunt, N. (2011). A new mechanism for ocean–atmosphere coupling in midlatitudes. *Quarterly Journal of the Royal Meteorological Society*, 137(657), 1095–1101.

Dee, D. P., Uppala, S. M., Simmons, A. J., Berrisford, P., Poli, P., Kobayashi, S., Andrae, U., Balmaseda, M. A., Balsamo, G., Bauer, P., Bechtold, P., Beljaars, A. C. M., van de Berg, L., Bidlot, J., Bormann, N., Delsol, C., Dragani, R., Fuentes, M., Geer, A. J., Haimberger, L., Healy, S. B., Hersbach, H., Hólm, E. V., Isaksen, L., Kållberg, P., Köhler, M., Matricardi, M., McNally, A. P., Monge-Sanz, B. M., Morcrette, J.-J., Park, B.-K., Peubey, C., de Rosnay, P., Tavolato, C., Thépaut, J.-N., & Vitart, F. (2011). The era-interim reanalysis: configuration

and performance of the data assimilation system. *Quarterly Journal of the Royal Meteorological Society*, 137(656), 553–597.

Flato, G., Marotzke, J., Abiodun, B., Braconnot, P., Chou, S. C., Collins, W., Cox, P., Driouech, F., Emori, S., Eyring, V., et al. (2013). Evaluation of climate models. In *Climate Change 2013: The Physical Science Basis. Contribution of Working Group I to the Fifth Assessment Report of the Intergovernmental Panel on Climate Change* (pp. 741–866). Cambridge University Press.

Giordani, H. & Caniaux, G. (2001). Sensitivity of cyclogenesis to sea surface temperature in the northwestern atlantic. *Monthly weather review*, 129(6), 1273–1295.

Haarsma, R. J., Hazeleger, W., Severijns, C., de Vries, H., Sterl, A., Bintanja, R., van Oldenborgh, G. J., & van den Brink, H. W. (2013). More hurricanes to hit western europe due to global warming. *Geophysical Research Letters*, 40(9), 1783–1788.

Hazeleger, W., Wang, X., Severijns, C., Ştefănescu, S., Bintanja, R., Sterl, A., Wyser, K., Semmler, T., Yang, S., Van den Hurk, B., et al. (2012). Ec-earth v2. 2: description and validation of a new seamless earth system prediction model. *Climate Dynamics*, 39(11), 2611–2629.

Jacobs, N., Raman, S., Lackmann, G., & Childs Jr, P. (2008). The influence of the gulf stream induced sst gradients on the us east coast winter storm of 24–25 january 2000. *International Journal of Remote Sensing*, 29(21), 6145–6174.

Jones, P. W. (1999). First-and second-order conservative remapping schemes for grids in spherical coordinates. *Monthly Weather Review*, 127(9), 2204–2210.

Joyce, R. J., Janowiak, J. E., Arkin, P. A., & Xie, P. (2004). Cmorph: A method that produces global precipitation estimates from passive microwave and infrared data at high spatial and temporal resolution. *Journal of Hydrometeorology*, 5(3), 487–503.

Ma, X., Chang, P., Saravanan, R., Montuoro, R., Hsieh, J.-S., Wu, D., Lin, X., Wu, L., & Jing, Z. (2015). Distant influence of kuroshio eddies on north pacific weather patterns? *Scientific reports*, 5.

Minobe, S., Kuwano-Yoshida, A., Komori, N., Xie, S.-P., & Small, R. J. (2008). Influence of the gulf stream on the troposphere. *Nature*, 452(7184), 206–209.

Reynolds, R. W., Smith, T. M., Liu, C., Chelton, D. B., Casey, K. S., & Schlax, M. G. (2007). Daily high-resolution-blended analyses for sea surface temperature. *Journal of Climate*, 20(22), 5473–5496.

Rienecker, M. M., Suarez, M. J., Gelaro, R., Todling, R., Bacmeister, J., Liu, E., Bosilovich, M. G., Schubert, S. D., Takacs, L., Kim, G.-K., et al. (2011). Merra: Nasa's modern-era retrospective analysis for research and applications. *Journal of Climate*, 24(14), 3624–3648.

Sheldon, L., Czaja, A., Vanniere, B., Morcrette, C., Casado, M., & Smith, D. (2016). "a warm path" to gulf stream-troposphere interactions. *in preperation, personal communication.*

Small, R. J., Tomas, R. A., & Bryan, F. O. (2014). Storm track response to ocean fronts in a global high-resolution climate model. *Climate dynamics*, 43(3-4), 805–828.

Stephens, G. L., L'Ecuyer, T., Forbes, R., Gettlemen, A., Golaz, J.-C., Bodas-Salcedo, A., Suzuki, K., Gabriel, P., & Haynes, J. (2010). Dreary state of precipitation in global models. *Journal of Geophysical Research: Atmospheres*, 115(D24), n/a–n/a. D24211.

van Haren, R., Haarsma, R. J., van Oldenborgh, G. J., & Hazeleger, W. (2015). Resolution dependence of european precipitation in a state-of-the-art atmospheric general circulation model. *Journal of Climate*, (2015).

Zappa, G., Shaffrey, L. C., & Hodges, K. I. (2013). The ability of cmip5 models to simulate north atlantic extratropical cyclones*. *Journal of Climate*, 26(15), 5379–5396.

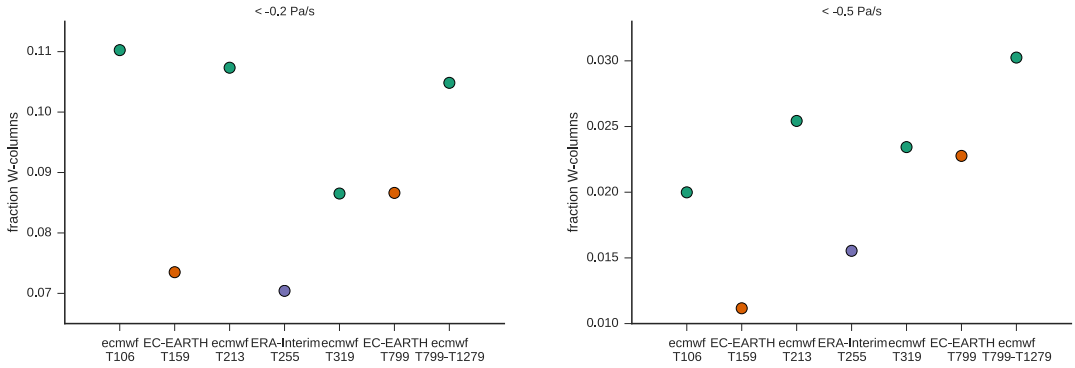

Figure 10: Fraction of wintertime deep convection events ($\omega <$ threshold from 850-300 hPa, details see text), with threshold -0.2 Pa/s (left) and -0.5 Pa/s (right), averaged over the study region. x-axis shows spectral horizontal resolution of the model/renalysis. ECMWF-operational (green, denoted ecmwf) was split up in four time-periods, corresponding to periods with a certain horizontal resolution. ERA-Interim (purple) and both resolutions of the EC-Earth experiment (red). Note that the x-axis is only categorical and not exactly scaled to horizontal resolution

Supplementary Material

Resolution Dependence of Deep Convection in ERA-Interim the ECMWF-operational Analysis

In section 3.3 we showed that the ECMWF-operational analysis from 2004 to 2014 (with a resolution of first T799 and later in the period T1279) shows a higher fraction of deep convection events than ERA-Interim and both resolutions of EC-Earth. If the analysis is expanded to all resolutions of the ECMWF-operational analysis separately (T106, T213, T319, T799), we get an on the first hand confusing picture. Fig. 10 shows the mean fraction of wintertime events of deep convection in the study-region for all ECMWF-operational resolutions, ERA-Interim and both resolutions of EC-Earth. Shown are the results for two thresholds of vertical velocity. We see that, in conclusion with our main findings, T319 shows less events than T799-T1279. Contrarily, T213 shows more events than T319. This can be explained by a change in the cloud scheme of the IFS model in 2003, which made the atmosphere more stable, with less vertical motion (Dee et al. 2011). This update falls in the middle of the period of T319. Therefore, the difference between T213 and T319 is affected by two opposing effects: the increase in resolution leads to more vertical motion - in conclusion with our findings - but this is overcompensated by the effect of the new cloud scheme, which causes less vertical motion. This also explains why ERA-Interim - with a resolution of T255- shows less deep convection events than all resolutions of ECMWF-operational. ERA-Interim uses the new (more stable) cloud scheme, but on a lower resolution than the versions of ECMWF-operational that also use the new cloud scheme. Therefore it is the only model with both the more stable cloud scheme, and low resolution - causing it to have the smallest fraction of deep convection events.

Part II

Influence of SST-Gradients on the Development of Mid-Latitude Storms

Key Points

- SST-gradients significantly influence development of midlatidude storms
- Huge spread in response from case to case, average response small
- No single explanation possible for responses of storms to differences in SST gradients

Abstract

In a controlled experiment with a regional climate model, we investigated the influence of strong SST-gradients in the Gulf Stream region on the development of a number of wintertime storms. We show that the removal of the SST-gradients significantly impacts the storms, with the number of weakening and strengthening storms roughly balancing each other. While one of the determining factors is the track of the storms with respect to the SST-front, we show that no single explanation is possible. Therefore, we propose two separate mechanisms that explain most of the responses. The first mechanism is related to latent heat flux, the second mechanism to baroclinicity.

1 Introduction

The Gulf Stream - characterized by its high SST-gradients and the warm-tongue extension - is one of the worlds major regions of mid-latitude storm development. It has long been hypothesized that the SST-gradients have a strong influence on the climate in this region, especially on storm development. Several studies have been conducted on the climatic impacts of SST-gradients in the Gulf Stream region. It has been shown that the Gulf Stream has a clear imprint on the atmosphere even at higher altitudes of the troposphere (Minobe et al., 2008). The presence of the Gulf Stream significantly impacts local precipitation and the storm track (Minobe et al., 2008; Small et al., 2014). The storm track is also influenced by insufficient spatial resolution of SST-fields representing the Gulf Stream (Piazza et al., 2015). Recently remote impacts of small-scale oceanic features on precipitation have been shown (Ma et al., 2015). Beside climatological studies, case studies on individual (or a small number of) storms have revealed first insights into the mechanisms causing the influence of SST-gradients on storm development (e.g.Booth et al. 2012; Giordani & Caniaux 2001; Jacobs et al. 2008; Sheldon et al. 2016). There are indications that both the absolute values of SSTs and the magnitude of the SST-gradient influence storm-development, with the absolute SST values being the more important driver, and latent heat release playing an important role (Booth et al., 2012).

This study aims to close the gap between the climatological studies and the single case studies. By simulating 27 individual cases, we want to investigate how storms are influenced by changes in SST-gradients, whether a “typical” response exists, and how well insights from single storms are valid for all (or the majority) of storms. In contrast to most case studies, we do not focus on especially strong storms or storms with a certain trajectory along or across the SST-front.

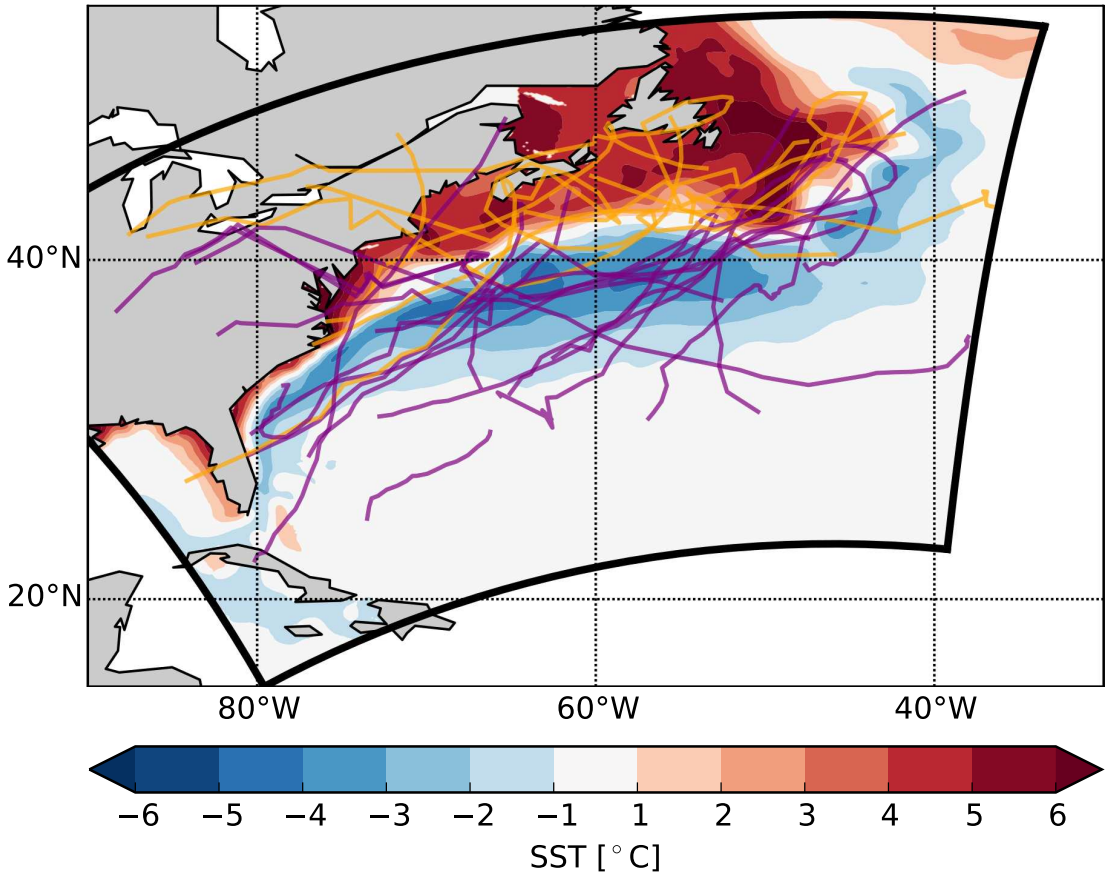

Figure 1: Tracks of the simulated storms. Yellow (purple) lines denote tracks that are on average north (south) of the SST-front. Contours: difference of SSTs (SMTH-REF) averaged over study period (NDJF 2006-2012). The black box denotes the domain of the regional simulation.

Our sole selection criterion is that the storms do travel over the Gulf Stream, originating both from land and ocean, and occur in extended winter (NDJF). The storms were selected with an automated tracking algorithm based on the one used by Blender et al. (1997). We used the ERA-interim dataset (Dee et al., 2011) for the periods 2006-2012 to detect the storms and as boundary condition. This resulted in 48 selected storms. Due to technical problems we were not able to simulate all selected storms, and finally used 27 separate storm-cases for our study. For each storm, we made a twin-simulation with the climate version of the regional weather forecasting model HARMONIE with hydrostatic physics and 10km horizontal resolution (Lindstedt et al., 2015). The twin simulations use the same lateral boundary conditions, but different underlying SST-fields. The reference run (REF) uses the NOAA 1/4° daily Optimum Interpolation Sea Surface Temperature data set (Reynolds et al., 2007), whereas the SMTH run uses the same SST-dataset, but with a smoothing algorithm applied. The smoothing algorithm first fills up land points with the latitudinal mean SST-values of the domain as pseudo-SSTs, and then applies a 3x3 gridpoint smoother 2000 times. This effectively removes the Gulf Stream warm extension and the strong SST-gradients along the Gulf Stream front. To ensure that the average SST in the domain does not change in the smoothing process, we subtracted the difference of the mean SST-value of the field between before and after the smoothing from the smoothed field to obtain the final field. The shading in fig. 1 shows the difference between the smoothed and the full resolution SST fields

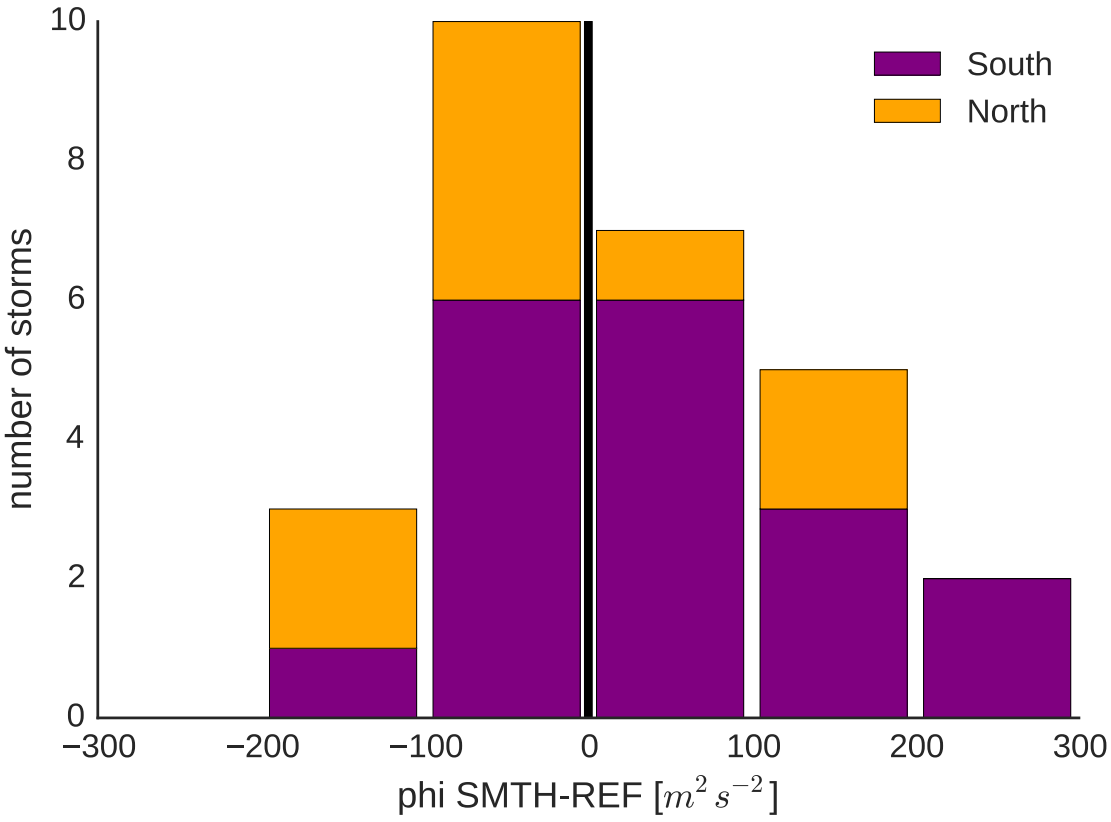

Figure 2: Differences in geopotential height of the 925 hPa surface between the SMTH and the REF runs averaged in a box of 30x30km around the track, grouped in storms that are on average north (yellow) or south (purple) of the SST-front.

(averaged over all storm cases). The smoothing results in a dipole-pattern, with increased SSTs north and decreased SSTs south of the SST-front. Fig. 1 also shows the tracks of all simulated storms. The thick black line marks the domain of the regional model. The domain was chosen to be rather small, encompassing only the region with strong SST-gradients. By choosing a small domain, the large scale baroclinicity is fed in through the boundaries, and therefore held constant. This allows us to disentangle the effects of changes in the large scale baroclinicity and effects of a more local nature. All effects that we observe in our experiment are therefore caused by regional processes, and not by changes in large scale circulation (which might occur in global simulations when using different SST-gradients as forcing).

2 Results

The trajectories of the storms were very similar for the REF and STMH simulations, being apparently mainly determined by the boundary conditions at the border of the domain. To determine the influence of initial conditions on the simulation, we reran one REF-simulation two times. One simulation was initialized 24 hours earlier and the other one 48 hours earlier than the standard REF-simulation. After one and a half days of overlapping time with the standard REF- simulation, the differences were very small compared to the difference with the SMTH-run. This reveals that the experiment is controlled by the boundary conditions which were continuously fed in at the border of the domain, and not by the initial state of the atmosphere. This makes our experiment

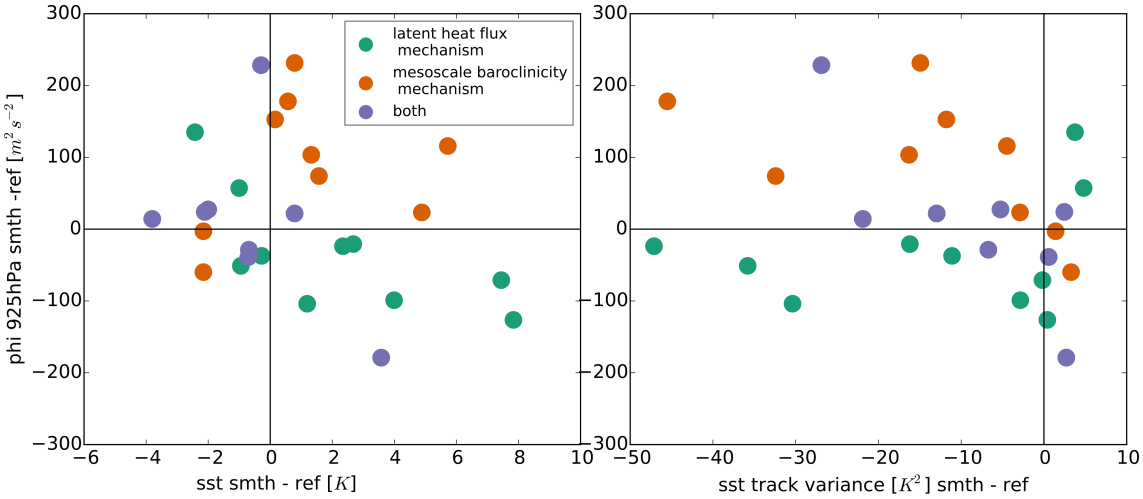

Figure 3: Relation between SST and phi925hPa (left) and SST-track-variance and pi925hPa (right). Definition of SST-track-variance see text. Each point denotes the difference between one SMTH and REF pair, averaged along the track. Green dots are proposed for mechanism 1 (Latent Heat Flux Mechanism), orange dots for Mechanism 2 (Mesoscale Baroclinicity Mechanism), and purple dots for both. phi925hPa was averaged in a box of 30x30km around the track, the other variables in a box of 100x100km.

more robust, as the exact time of the start of the simulation is thus not crucial for the outcome.

To investigate the results of our experiment, we developed an along-track measure that summarizes the response of a chosen variable (e.g. wind speed) to the smoothing of the SSTs. For this, we first determine the center of the storm as the local minima of the geopotential height at 925hPa (phi925hPa) for every 6-hour timestep, which results in an exact track of the storm. The tracking was done for both the REF and SMTH runs separately to account for small deviations in the tracks. Then the variable is averaged over a box around the center of the storm, which results in a single timeline for each variable. The size of the box varies from variable to variable and is mentioned in the respective figure captions. In the next step, the timeline is averaged over time, which results in a single value for the simulation. In the last step, the difference between this value for the SMTH and the value for the REF simulation is computed, providing a single number for the impact of the SST-smoothing on the respective variable.

When applying this metric on phi925hPa, about half of the storms show a weakening (increase of phi925hPa), and the other half a strengthening of the storm (decrease of phi925hPa) as a response to SST-smoothing (fig. 2). We now tried to investigate the cause of this mixed response. First we grouped the storms according to whether they spend their average lifetime north (south) of the strong SST-front, and colored them yellow (purple) in fig. 1 and 2. This revealed that the groups are not equal in terms of the response of the averaged depression strength to SST-smoothing. The storms south of the front more tend to weaken, whereas the storms north of the front more tend to strengthen as a response to SST-smoothing.

For further investigation we developed a measure for the "smoothness" of the underlying SSTs along the track. For this we first computed the average SST in a box (100 by 100 km) around each track-point. We then calculated the variance of this timeseries. This provides a measure of how much the SSTs change along the track, and will be denoted as SST-track variance further on. Fig. 3 shows the relations of the differences between the SMTH and REF runs for the variables phi 925hPa, SST and SST-track variance, all averaged along the track. The left panel in fig 3 (phi

vs SST) suggests that there is a connection between difference in average SST and difference in phi 925hPa, if not for all points, so at least for some of them. The right panel suggests something similar for SST track variance and phi 925hPa, again not for all, but for some storms. We colored all points in the upper left and lower right quadrants of the left panel in green (implying a negative correlation between difference in average SST and phi925hPa). The same quadrants in the right panel were colored in orange (implying a negative correlation between sst track variance and phi 925hPa). Storms falling in both categories were colored purple. Close to the origin we relaxed our selection criterion, allowing also storms in the "wrong" quadrants to be selected if they are no farther away from the origin than one half of the standard deviation of the variables on the respective axes. The reasoning behind this is that nearly no change in e.g. SST paired with nearly no change in phi925hPa is in congruence with a negative correlation. We see that some storms are subject to either one correlation, and some to both. Remembering that the differences in SST and SST track variance are prescribed in our experiment - they are therefore predictors - this suggests that there are two separate physical mechanisms causing the changes between the SMTH-REF twins in our experiment. They will be discussed below.

2.1 Latent Heat Flux Mechanism

The upper left panel in fig. 4 shows differences of SST vs differences of LHF between all SMTH and REF runs. There is a clear positive correlation between the difference in the average SST the storm "sees" and the difference in the amount of latent heat flux from the ocean to the atmosphere. Based on this we propose the following mechanism acting on all green and purple storms, illustrated by a storm that "sees" on average colder SSTs due to the smoothing: If the SSTs are colder, there is less latent heat flux. Therefore, the storm loosens one of its driving forces (the other being baroclinicity) and gets weaker compared to the REF simulation, where SSTs are on average higher. Figure 4 shows the relation between the difference in latent heat flux and total precipitation (upper right panel) and Convective Available Potential Energy (CAPE) (lower left panel). Note that there are two outliers (high positive change in CAPE) that are not shown. These are caused by very low values of CAPE in the REF run, and accordingly high relative change. We see that there is a weak correlation between LHF and TP, with more LHF leading to more precipitation, which drives the storm via latent heat release. The weakness of this correlation can be explained by remembering that LHF does not always directly (and especially not instantaneously) lead to precipitation, and that water vapor can also be transported into the area where it precipitates, being caused by evaporation elsewhere in space and in time.

A better correlation exists between the difference in CAPE and LHF, which indicates that more LHF leads to a more unstable atmosphere via moistening of the lower layers of the atmosphere - and therefore, increasing CAPE. This will enhance convection, which will cause enhanced wind convergence and a strengthening of the storm. A similar mechanism has been suggested in a case-study by Sheldon et al. (2016), where convection in the warm sector of a storm that passes directly over the Gulf Stream warm extension decreases significantly with smoothed SSTs. With these insights - and realizing that the same mechanism works in the opposite direction if the SSTs do not get colder but warmer through smoothing - we can summarize our first mechanism: colder (warmer) SSTs along the track lead to less (more) latent heat release, which makes the lower layers of the atmosphere less (more) moist and thus the whole atmosphere more (less) stable, leading to a weaker (stronger) driving of the storm and finally a decrease (increase) of the depth of the depression. It has to be noted that the relations discussed here are not only valid for the cases proposed for the Latent Heat Flux Mechanism (green and purple), but also for the rest of the

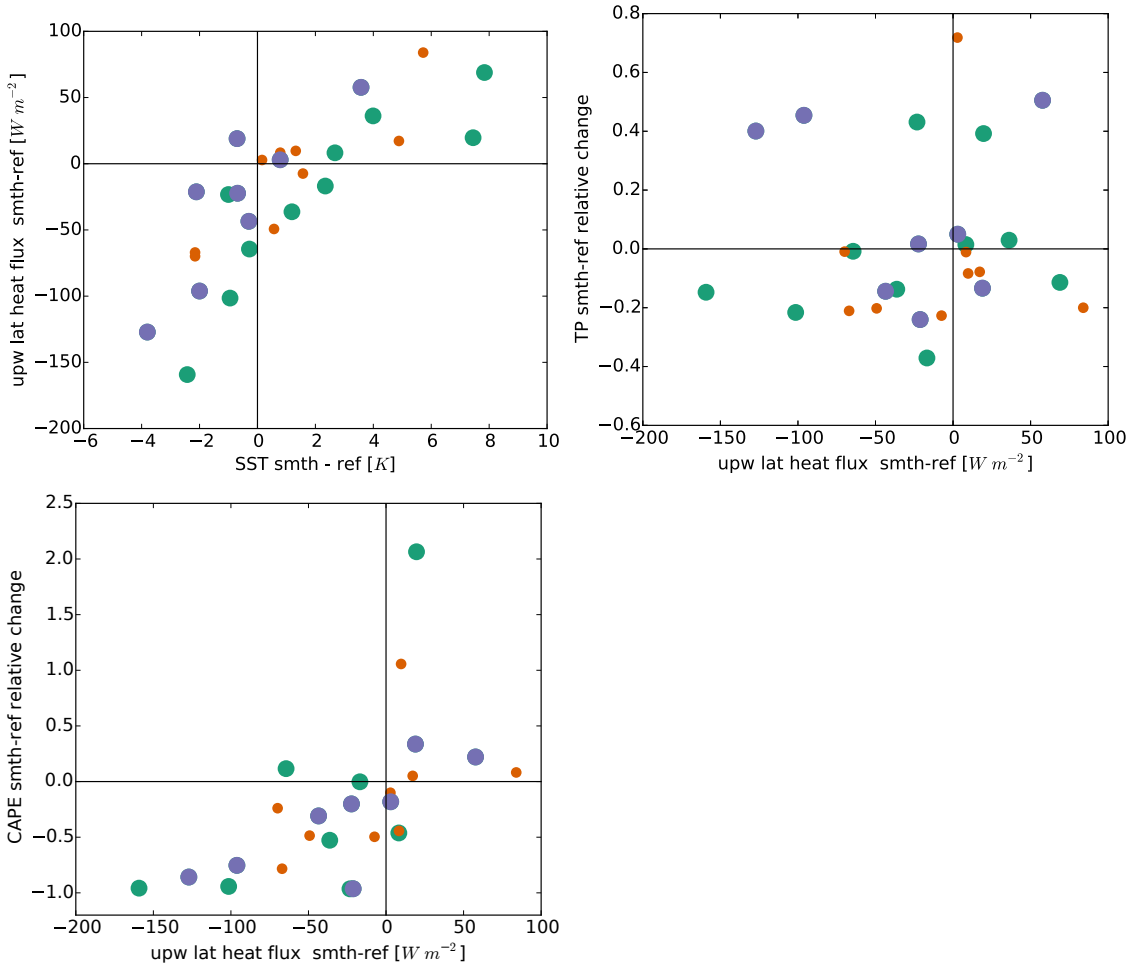

Figure 4: Testing of the Latent Heat Flux Mechanism. Relation between SST and LHF above sea (upper left), LHF above sea and relative change of total precipitaton (upper right) and LHF above sea and change in CAPE (lower left). Each point denotes the difference between one SMTH and REF pair, averaged in a box 110x110km along the track. Storms subject to the Latent Heat Flux Mechanism are highlighted by larger points. The lower left panel has two outliers (high positive change in CAPE) that are not shown. Colors as in fig. 3.

cases. Thus, this mechanism is acting also on the red storms, but the resulting signal of change in phi 925hPa is not as expected. Therefore, there must be a second mechanism, overpowering the first mechanism in these cases.

2.2 Mesoscale Baroclinicity Mechanism

While the Latent Heat Flux mechanism can explain the green and purple colored storms, it cannot explain the storms in the upper right (lower left) quadrant in the upper left panel of fig. 3. These storms see on average warmer (colder) SSTs, but get weaker (stronger) in response to SST-smoothing. Therefore, we propose a second mechanism, starting from the difference in along-track SST variance. This difference in the "smoothness" or "sharpness" of SSTs causes changes in the baroclinicity (lowering it if the track variance decreases). We used the Eady Growth Rate (definition see Appendix) at 700hPa as a measure of baroclinicity, averaged over the whole domain. In the left panel of fig. 5 the change in SST-track variance is plotted against the relative change in

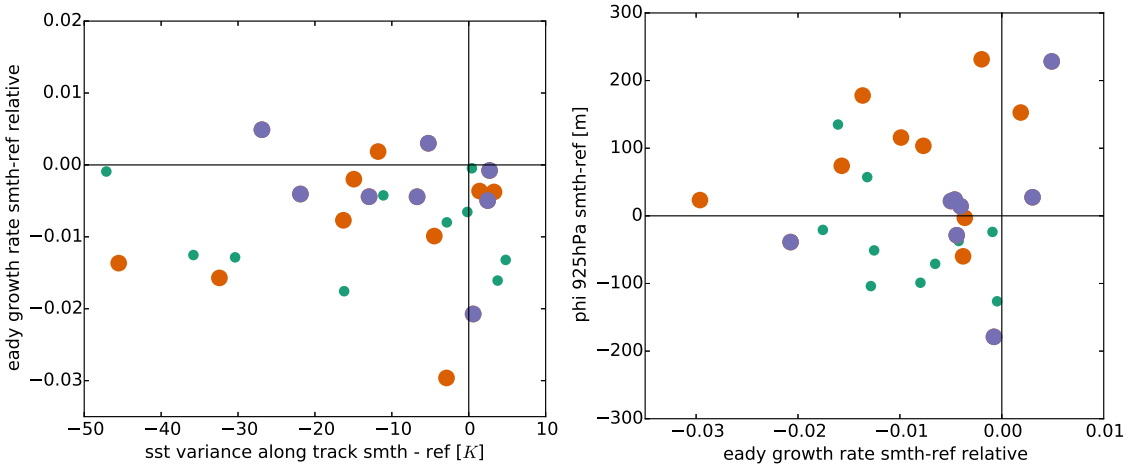

Figure 5: Testing of the Mesoscale Baroclinicity Mechanism. Relation between sst track variance and Eady Growth Rate (sigma) (left panel) and between the Eady Growth Rate and phi925hPa (right panel). Each point denotes the difference between one SMTH and REF pair. Storms subject to the Mesoscale Baroclinicity Mechanism are highlighted by larger points. phi925hPa and sst track variance as in fig.3, Eady Growth rate averaged over the whole domain. Colors as in fig. 3

Eady growth rate. A negative value corresponds to a decrease in baroclinicity. It can be seen that most orange and green points lie in the lower left quadrant, showing a positive correlation between SST-track variance and baroclinicity. In the right panel of the figure the relative change in Eady Growth rate is plotted against the change in phi 925hPa. We see that the majority of orange and purple points lies in the two quadrants indicating negative correlation. Based on these findings, we propose the second mechanism as follows: lower SST track variance leads to a change in the temperature structure of the atmosphere, making it less baroclinic. Therefore, the major driver for the formation of depressions is reduced, and the storm gets weaker.

2.3 Case Study

We saw in the previous sections that the latent heat flux mechanism contributes to all storms. Therefore, we further investigate and illustrate this mechanism on the basis of one example storm. The right panel of fig. 6 shows the evolution of SST, LHF, phi925hPa, temperature at 2m and precipitation along the tracks of the REF and the SMTH run. The left panel shows a snapshot of the REF-windspeed averaged over 18 hours around the occurrence of the phi-minimum in the REF run (upper left), and the difference between windspeed of the SMTH and REF run around the same point in time (lower left). We see that the storm in SMTH run starts at the same values of SSTs as the REF-run, but as the storm propagates, it travels over much colder ($\sim 5K$) SSTs than the REF run. This difference in SSTs is - although with a damping of the magnitude - communicated to the lower layer of the atmosphere, visible in the 2m temperature. Therefore the temperature difference between the ocean surface and the lower atmosphere is lower in the SMTH run, which results in less surface latent heat flux. Whereas the REF run experiences a strong peak of latent heat flux 10 hours prior to its maximum depression, this peak in LHF is absent in the SMTH run. This reduced heat flux manifests itself in a weaker depression in the SMTH run, and reduced wind-speeds (on the order of 2-4 m/s) - thus a weakening of the storm. The time-evolution of precipitation is more chaotic, but integrated over the track, the SMTH runs shows 14% less precipitation than the REF run, which is in congruence with our mechanism. Note that the SST-track variance is higher in

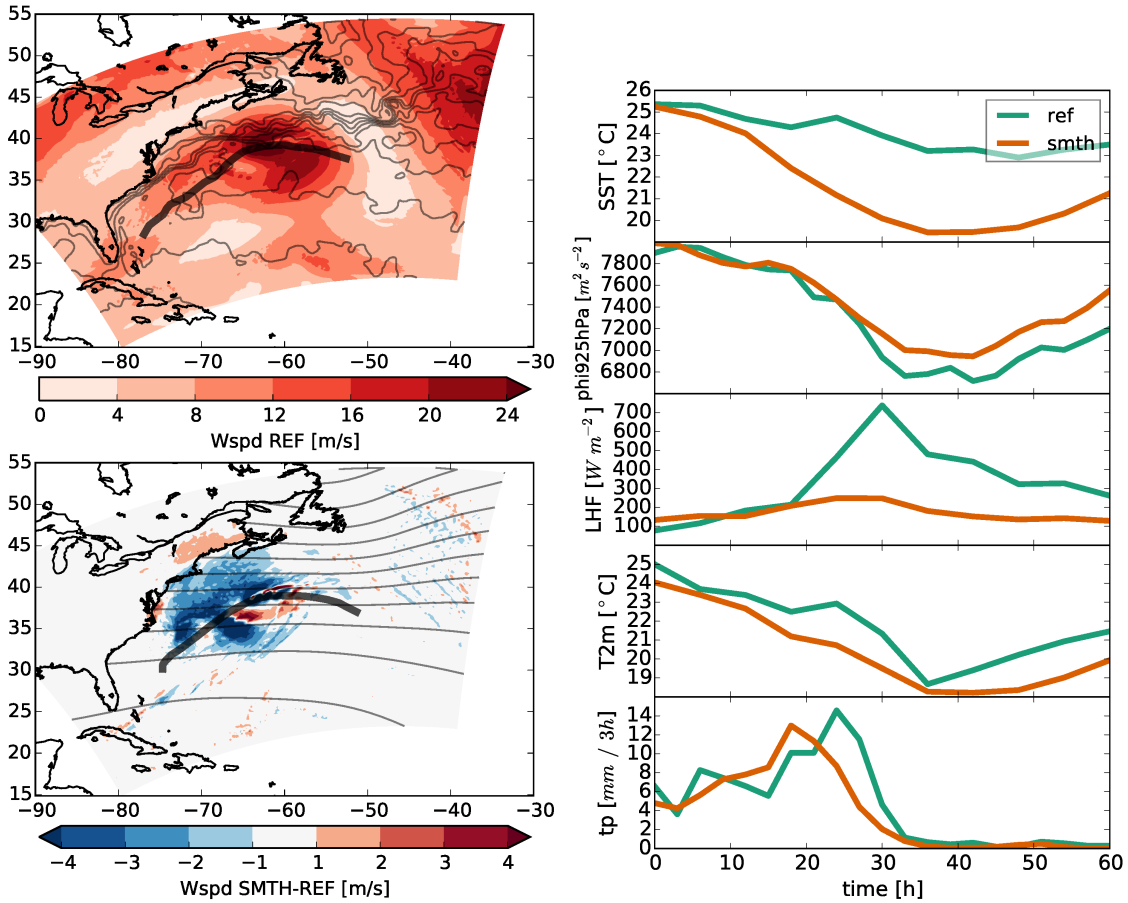

Figure 6: Left: Windspeed at 925hPa of the REF run (upper left) and SMTH minus REF (lower left) of one case, averaged over 18 hours centered around the time of the occurrence of the minimum of phi925 in the REF-run. Right: Timelines of SST, phi925hPa, LHF above sea, temperature at 2m (T2m) and precipitation (tp) of the same storm. The values are averaged over a box of 100x100 km around the current position on the track (the latter is denoted by the thick black line in the left panels). The contour lines in the left panels denote the average SSTs of the REF run (upper left) and SMTH run (lower left), with 2K spacing.

the SMTH run - the REF storm "sees" nearly constant SSTs, whereas the SMTH run experiences a strong dip in SSTs. This further confirmed the idea brought forward by Sheldon et al. (2016) - namely that not so much the gradient, but the existence of the Gulf Stream warm tongue, and the resulting warmer SST-path along the track - help storms to intensify.

3 Discussion

While the two mechanisms we proposed give insight into the physical processes behind the response of most storms to SST-smoothing, they cannot explain all cases. For this a detailed investigation of each storm case would be necessary, which is beyond the scope of this study. Additionally, the second mechanism (Mesoscale Baroclinicity) is less robust than the first mechanism (latent heat flux), as the correlations between the steps in our reasoning are weaker. Nevertheless we argue that we are able to provide a first physical reasoning of the of the responses of a large number of storms to changes in SST-gradients. It might also be the case that some small scale effects (e.g.

convection) can only be covered at finer resolution and with non-hydrostatic physics, which future studies will have to investigate.

4 Summary and Conclusions

We showed with regional simulations of 27 storms that SST-gradients do have a significant influence on the development of midlatitude storms above the Gulf Stream, and that the response of individual storms to changes of SST-gradients is manifold. The main determining factor seems to be the differences of SSTs along the track of the storm, which causes the response to be determined by whether the smoothing will make the SSTs the storm "sees" on average warmer or colder. Storms that pass north of the Gulf Stream SST-front experience warmer SSTs when applying smoothing, storms south of the front experience colder SSTs. We proposed two separate physical mechanisms causing the responses of the individual storms to changes in the underlying SSTs. The first mechanism - the "latent heat flux mechanism"- directly communicates the change of SSTs along the track via changes in latent heat flux, which affects the development of the storms via latent heat release and changes of the stability of the atmosphere. This mechanism could satisfactorily be confirmed by analyzing one of the storms in detail, and is in congruence with the findings by Sheldon et al. (2016). This mechanism is able to explain around half of our storm cases.
Secondly we proposed a "mesoscale baroclinicity mechanism" that attempts to explain the cases that cannot be explained by the first mechanism. This mechanism links the SST-gradients in the larger vicinity of the storm to upper atmosphere baroclinicity, which is the main driver for the development of depressions. While a thorough confirmation of this mechanism was not possible, we still argue that this mechanism plays a dominant role in some and a supporting role in others of our cases.

Our overarching result is that storms do both weaken and strengthen as a response to the removal of the Gulf Stream, with the number of storms weakening and the number of storms strengthening roughly balancing each other. We remember that the setup of our experiment held the large scale baroclinicity fixed. Therefore, we argue that, even though we do not have a complete representative sample of storms, the weakening of the storm track when smoothing the Gulf Stream in GCMs (Piazza et al., 2015; Small et al., 2014) is mainly not caused by local or mesoscale effects - like the two mechanisms proposed in our study - but by changes in the large scale circulation, which further cause changes in the large scale baroclinicity and therefore changes the storm track.

The present study is, to the knowledge of the authors, the first study that analyses the influence of SST-gradients in a controlled experiment not with only one or a small number of storms, but with a larger sample. The considerable spread in the responses of our storms shows that results from single case studies have to be interpreted with care. While one single case might show a strong response that can be explained by physical reasoning (e.g. via latent heat release and changes in convection as in Sheldon et al. (2016)), this might not be representative for storms in general, and extrapolation from single cases to climatological changes due to different SST-forcings are therefore not possible.
Further our results show that a good representation of SST-fields is necessary for correctly modeling storms, which has consequences for the accurateness of numerical weather prediction and local climate simulations.

Appendix

Definition of Eady Growth Rate

The Eady Growth rate σ is defined on pressure coordinates as

$$\sigma = 0.31 \cdot \frac{g}{N} \left| \frac{\nabla \theta}{\theta} \right|$$

with the buoyancy frequency

$$N^2 = -g^2 \frac{\rho}{\theta} \frac{\partial \theta}{\partial p}$$

where g is is the gravitational acceleration of the Earth, θ is the potential temperature, ρ the density of the air, p the air pressure and ∇ the horizontal gradient operator.

References

Blender, R., Fraedrich, K., & Lunkeit, F. (1997). Identification of cyclone-track regimes in the north atlantic. *Quarterly Journal of the Royal Meteorological Society*, 123(539), 727–741.

Booth, J. F., Thompson, L., Patoux, J., & Kelly, K. A. (2012). Sensitivity of midlatitude storm intensification to perturbations in the sea surface temperature near the gulf stream. *Monthly Weather Review*, 140(4), 1241–1256.

Dee, D. P., Uppala, S. M., Simmons, A. J., Berrisford, P., Poli, P., Kobayashi, S., Andrae, U., Balmaseda, M. A., Balsamo, G., Bauer, P., Bechtold, P., Beljaars, A. C. M., van de Berg, L., Bidlot, J., Bormann, N., Delsol, C., Dragani, R., Fuentes, M., Geer, A. J., Haimberger, L., Healy, S. B., Hersbach, H., Hólm, E. V., Isaksen, L., Kållberg, P., Köhler, M., Matricardi, M., McNally, A. P., Monge-Sanz, B. M., Morcrette, J.-J., Park, B.-K., Peubey, C., de Rosnay, P., Tavolato, C., Thépaut, J.-N., & Vitart, F. (2011). The era-interim reanalysis: configuration and performance of the data assimilation system. *Quarterly Journal of the Royal Meteorological Society*, 137(656), 553–597.

Giordani, H. & Caniaux, G. (2001). Sensitivity of cyclogenesis to sea surface temperature in the northwestern atlantic. *Monthly weather review*, 129(6), 1273–1295.

Jacobs, N., Raman, S., Lackmann, G., & Childs Jr, P. (2008). The influence of the gulf stream induced sst gradients on the us east coast winter storm of 24–25 january 2000. *International Journal of Remote Sensing*, 29(21), 6145–6174.

Kuo, Y.-H., Low-Nam, S., & Reed, R. J. (1991). Effects of surface energy fluxes during the early development and rapid intensification stages of seven explosive cyclones in the western atlantic. *Monthly Weather Review*, 119(2), 457–476.

Lindstedt, D., Lind, P., Kjellström, E., & Jones, C. (2015). A new regional climate model operating at the meso-gamma scale: performance over europe. *Tellus A*, 67.

Ma, X., Chang, P., Saravanan, R., Montuoro, R., Hsieh, J.-S., Wu, D., Lin, X., Wu, L., & Jing, Z. (2015). Distant influence of kuroshio eddies on north pacific weather patterns? *Scientific reports*, 5.

Minobe, S., Kuwano-Yoshida, A., Komori, N., Xie, S.-P., & Small, R. J. (2008). Influence of the gulf stream on the troposphere. *Nature*, 452(7184), 206–209.

Piazza, M., Terray, L., Boé, J., Maisonnave, E., & Sanchez-Gomez, E. (2015). Influence of small-scale north atlantic sea surface temperature patterns on the marine boundary layer and free troposphere: a study using the atmospheric arpege model. *Climate Dynamics*, (pp. 1–19).

Reynolds, R. W., Smith, T. M., Liu, C., Chelton, D. B., Casey, K. S., & Schlax, M. G. (2007). Daily high-resolution-blended analyses for sea surface temperature. *Journal of Climate*, 20(22), 5473–5496.

Sheldon, L., Czaja, A., Vanniere, B., Morcrette, C., Casado, M., & Smith, D. (2016). "a warm path" to gulf stream-troposphere interactions. *in preperation, personal communication.*

Small, R. J., Tomas, R. A., & Bryan, F. O. (2014). Storm track response to ocean fronts in a global high-resolution climate model. *Climate dynamics*, 43(3-4), 805–828.